AIP | APL Materials

Reduced graphene oxide and Ag wrapped TiO2 photocatalyst for enhanced visible light photocatalysis

Kah Hon Leong, Lan Ching Sim, Detlef Bahnemann, Min Jang, Shaliza Ibrahim, and Pichiah Saravanan

Citation: APL Mater. **3**, 104503 (2015); doi: 10.1063/1.4926454
View online: http://dx.doi.org/10.1063/1.4926454
View Table of Contents: http://scitation.aip.org/content/aip/journal/aplmater/3/10?ver=pdfcov
Published by the AIP Publishing

Reduced graphene oxide and Ag wrapped TiO_2 photocatalyst for enhanced visible light photocatalysis

Kah Hon Leong,[1] Lan Ching Sim,[1] Detlef Bahnemann,[2] Min Jang,[1] Shaliza Ibrahim,[1] and Pichiah Saravanan[1,3,a]

[1]*Environmental Engineering Laboratory, Department of Civil Engineering, Faculty of Engineering, University of Malaya, 50603 Kuala Lumpur, Malaysia*
[2]*Institut fuer Technische Chemie, Leibniz Universität Hannover, Callinstrasse 3, D-30167 Hannover, Germany*
[3]*Nanotechnology & Catalysis Research Center (NANOCAT), University of Malaya, 50603 Kuala Lumpur, Malaysia*

(Received 21 April 2015; accepted 24 June 2015; published online 21 July 2015)

A well-organised reduced graphene oxide (RGO) and silver (Ag) wrapped TiO_2 nanohybrid was successfully achieved through a facile and easy route. The inherent characteristics of the synthesized RGO-Ag/TiO_2 were revealed through crystalline phase, morphology, chemical composition, Raman scattering, UV-visible absorption, and photoluminescence analyses. The adopted synthesis route significantly controlled the uniform formation of silver nanoparticles and contributed for the absorption of light in the visible spectrum through localized surface plasmon resonance effects. The wrapped RGO nanosheets triggered the electron mobility and promoted visible light shift towards red spectrum. The accomplishment of synergised effect of RGO and Ag well degraded Bisphenol A under visible light irradiation with a removal efficiency of 61.9%. [http://dx.doi.org/10.1063/1.4926454]

In recent years, the rapid growth of industrialization mainly on the manufacturing of polycarbonates to produce bottles, beverage containers, and electrical equipment contributed for the production of Bisphenol A (BPA).[1,2] It is a well-known micropollutant and classified as Endocrine Disrupting Compound (EDC) that is capable to impose adverse environmental and health effects due to its high toxicity.[3] Therefore, it drives most researchers to develop an effective alternative economical method for its safe disposal. Although many methods were reported, the photocatalytic oxidations process emerged as more significant over the rest.[4–6] It is well established that this process dominantly employs TiO_2 semiconductor owing to its high synergetic oxidation strength, zero toxicity, and greater chemical and biological stability.[7–9] In spite, it has major obstruction with wider bandgap energy (3.2 eV) and allows the photoactivation to only in the UV spectrum ($\lambda < 390$ nm). It also possess very low lifetime for the charge carriers and leads to a faster recombination rate.[10,11] Many researchers had attempted to overcome these limitations through doping with metals and non-metals, hetero-structures, noble metal, etc.[12–16] Considering noble metal as a potential impurity turned out to be an alternative approach for reconstructing the weaknesses of TiO_2.[17,18]

Further to improve the optical absorption and enhancing the charge carrier transport, reduced graphene oxide (RGO) was used in the hybrids thus narrows the bandgap and minimize the electron-hole recombination rate.[19] This is due to its rich characteristics in exhibiting high thermal conductivity, great charge carrier mobility, good surface contact with supported nanoparticles (NPs), and high hydrophobicity.[20–25] In addition, the spacious delocalized π-bond in the sp^2–bonded carbon lattice has enhanced its structure stability and conductivity capacity.[20,26] There are few reports that demonstrate the contribution of RGO and Ag towards visible light enhancement.[19,25,27]

[a]E-mail: pichiahsaravanan@gmail.com. Tel.: 0061-03-79677678. Fax: 0061-03-79675318.

Moreover, in order to explicit insight dominance and influence towards visible light utilization herein, we synergise localized surface plasmon resonance (LSPR) phenomenon, electrical properties, and surface science that lead to a highly efficient visible light activated photocatalyst (RGO-Ag/TiO_2). The improved visible light utilization of the developed photocatalyst was examined by degrading Bisphenol A under artificial visible light excitation.

Titanium (IV) chloride ($TiCl_4$, 99.9%, Merck), graphite flakes and silver nitrate ($AgNO_3$, 99.9%, Sigma Aldrich), tetrahydrofuran (THF, Fluka), ethylene glycol and benzyl alcohol (99.8% anhydrous), potassium permanganate ($KMnO_4$, 99.9%), sulfuric acid (H_2SO_4, 98%), hydrogen peroxide (H_2O_2, 30%), hydrogen chloride (HCl, 37%), and denatured ethanol (99.7%, R&M Chemicals) and Milli-Q water. All chemicals were analytically graded and used without any further modification.

Simplified Hummers method was adopted in synthesis of graphite oxide.[28] The detailed synthesis procedure is described in the supplementary material.[29] The synthesis of TiO_2 and Ag/TiO_2 was obtained from our previous studies.[16,30] The RGO was achieved by dissolving 0.2 g of synthesized GO in Milli-Q water under ultrasonic condition for an hour. The wrapping was succeeded by adding 1 g of the prepared Ag/TiO_2 into the yellow-brown solution (GO solution) and stirred for 1 h until a homogeneous phase appeared. This homogeneous solution was then autoclaved at 180 °C for 6 h. This hydrothermal treatment reduces GO to RGO. The resulted suspension was retrieved through centrifugation and washed thoroughly with Milli-Q water and dried at room temperature. The diagram of adopted synthesize route is illustrated in Fig. S1 of the supplementary material.[29]

The physical structure of the samples was investigated by Field Emission Scanning Electron Microscope (FESEM) at an accelerating voltage of 20 kV (Hitachi SU-8000). The particles size and lattice fringe images were identified through HRTEM (JEM-2100F, Jeol). The crystalline phase composition and grain size were studied with XRD of Bruker D8 Advance X-ray powder diffractometer with CuKα radiation λ = 0.154 nm. The Raman and photoluminescence (PL) spectra was acquired by using a micro-PL/Raman spectroscope of Renishaw with the excitation wavelengths at 514 nm and 325 nm, respectively. The functional group identification was carried out with FTIR obtained through Perkin Elmer Spectrum 400 spectrophotometer with a scan range of 4000-450 cm^{-1}. Chemical elemental species mapping and identification were obtained with XPS of Axis Ultra DLD instrument of Kratos, using monochromatic AlKα radiation (225 W, 15 mA, and 15 kV) and C 1s binding energy 284.9 eV as reference. The visible light harvesting characteristics were studied with Shimadzu UV-2600 spectrophotometer equipped with an integrating sphere attachment and used $BaSO_4$ as a reference.

The photocatalysis ability of the synthesized photocatalysts was demonstrated by degrading a poor photosensitizing compound, BPA. All the photocatalytic degradation experiments were carried using a 500 ml borosilicate beaker with a working volume of 250 ml. The initial concentration of BPA was maintained at 20 mg/l with 1 g of the prepared photocatalysts under continuous stirring conditions. A 500 W tungsten-halogen lamp with a high-pass UV filter (FSQ-GG400, Newport Corp) was used as an active photon energy source. All the experiments were carried out in an identical condition with 1 h dark reaction followed by 5 h photodegradation. Bisphenol A residuals were drawn out at regular interval, analyzed using a liquid chromatography (Acquity UPLC H-Class, Waters) mounted with C18 column (2.1 × 50 mm and 1.7 μm) at 40 °C employing water: ACN (60:40) as mobile phase with a flow rate of 0.4 ml/min. The targeted compound was quantified with a detection wavelength of 226 nm.

The transition of the photogenerated electrons in the composites was measured using a Metrohm Autolab (PGSTAT302N). A standard three-electrode system using platinum wire as counter electrode, Ag/AgCl as reference electrode, and indium-tin oxide (ITO) glass as working electrode was employed for the study. A tungsten-halogen lamp of 500 W with a high-pass UV filter was used as visible light source. An aqueous solution of 0.1M Na_2SO_4 was used as the electrolyte solution. As for the working electrodes, 5.0 mg of composite is dispersed in 1 ml ethanol and then dropped onto the pretreated ITO and air dried.

Fig. 1 illustrates the FESEM images of the successfully wrapped RGO and Ag with TiO_2. The image (Fig. 1(a)) clarifies the uniform distribution of Ag/TiO_2 onto the RGO sheets and (Fig. 1(b))

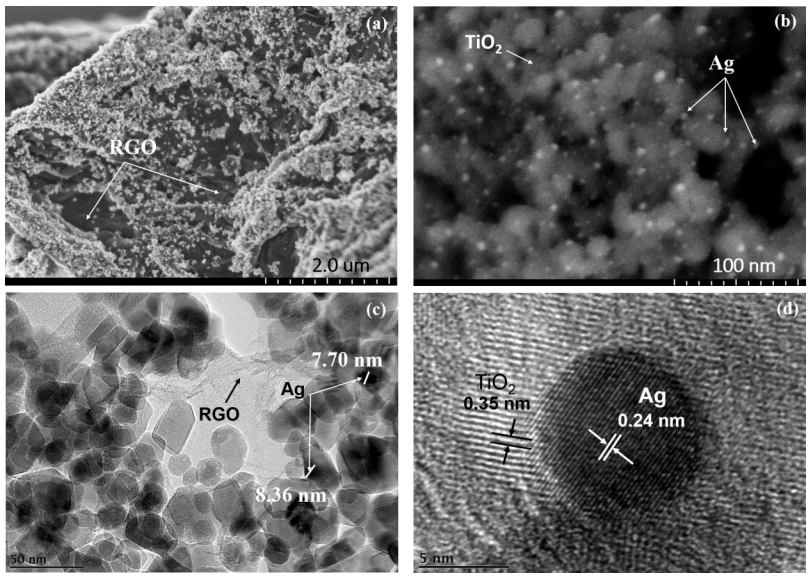

FIG. 1. Physical surface structural and composition images of the ((a) and (b)) RGO-Ag/TiO_2 and ((c) and (d)) HRTEM images of RGO-Ag/TiO_2.

Ag NPs onto the surface of TiO_2 trough by efficient sustainable photodeposition method. The particle size of Ag NPs with a lattice fringes spacing was detailed in Figs. 1(c) and 1(d).[31,32] FESEM and HRTEM images of pure TiO_2 and Ag/TiO_2 are shown in the supplementary material as Figs. S2(a) and S2(b) and S3(a) and S3(b), respectively.[29]

The diffraction pattern of RGO-Ag/TiO_2 is depicted in Fig. 2(A) along with the GO, TiO_2, and RGO-TiO_2. The diffraction peaks at $2\theta = 38.1°$, 44.3°, 64.4°, and 77.4° corresponded to crystal phases (1 1 1), (2 0 0), (2 2 0), and (3 1 1) of silver NPs, respectively (JCPDS No. 04-0783). The intense diffraction peaks also confirm the stability of the synthesized silver NPs. Meanwhile, a diffraction peak at $2\theta = 10.6°$ (0 0 2) was seen for GO sample signifying almost complete oxidation of nature graphite into GO by expanding the d-spacing from 0.34 to 0.93 nm.[10,33] The RGO did not show a notable diffraction peak in both RGO-TiO_2 and RGO-Ag/TiO_2, due to low amount of carbon species in the composites.[27,34,35] The average crystalline size TiO_2 in the ternary calculated using Scherrer equation was found to be 20.29 nm almost equivalent to the pure one (19.68 nm). The observed Miller indices for TiO_2 revealed the complete anatase phase of TiO_2.

The obtained Raman spectrum as shown in Fig. 2(B) portraits distinct peaks that attribute to anatase phase of TiO_2. Besides that, the inset of Fig. 2(B) shows the Raman spectrum of GO with two intense peaks at 1351 cm^{-1} (D-band) and 1605 cm^{-1} (G-band). The D-band attributed to the

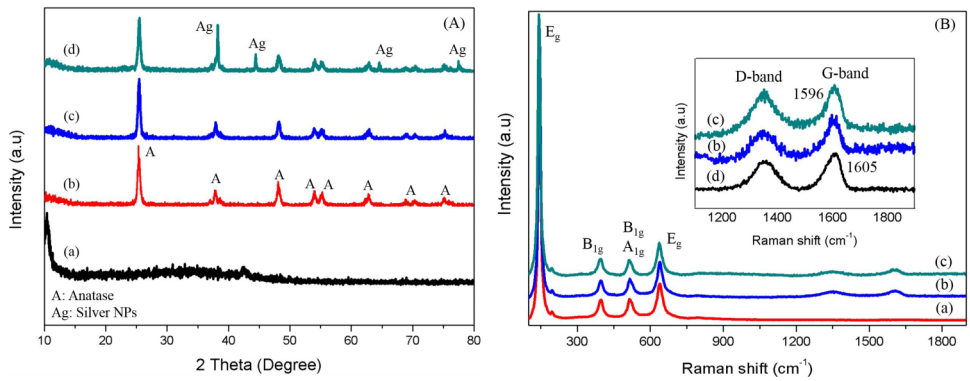

FIG. 2. (A) Diffraction patterns of (a) GO, (b) TiO_2, (c) RGO-TiO_2, and (d) RGO-Ag/TiO_2. (B) Raman spectra of (a) TiO_2, (b) RGO-TiO_2, (c) RGO-Ag/TiO_2 and inset is the (d) GO.

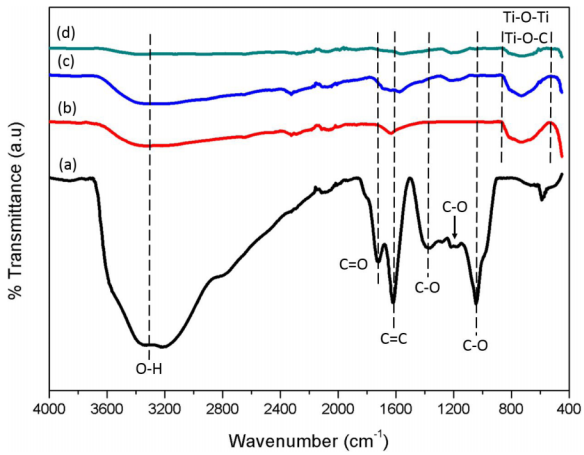

FIG. 3. Functional group spectra of (a) GO, (b) TiO_2, (c) RGO-TiO_2, and (d) RGO-Ag/TiO_2.

disorder with structural imperfections created during the reduction of GO. Meanwhile, the G-band corresponds to the first order scattering of E_{2g} photon of sp^2 C atoms of graphene.[25] Therefore, the intensity ratio (I_D/I_G) for GO was 0.78 signifying the presence of large amount of sp^3 in the sample. The D and G-bands of RGO-TiO_2 and RGO-Ag/TiO_2 were approximately in the same position with GO. However, the I_D/I_G ratio of RGO-TiO_2 (0.95) and RGO-Ag/TiO_2 (0.97) increased from 0.78 for GO, demonstrating the reduction of GO via hydrothermal process. This increment was carried through removal of oxygenated groups leading to re-establishment of conjugated graphene network.[36] The analysis further verified the charge transfer between GO and the hybridized components. This was observed in the G-band of GO having a marginal shift of ~9 cm^{-1} to a lower frequency at 1596 cm^{-1} (RGO-Ag/TiO_2) from 1605 cm^{-1} (GO) confirms the charge transfer between TiO_2 and RGO.[37]

The functional group spectra are illustrated in Fig. 3. The GO displayed many strong absorption peaks that correspond to various oxygen functional groups. The absorption peaks included the wide broad peak at 3400 cm^{-1} which correspond to the O—H stretching. The carboxylates C═O stretching occurred at peak 1730 cm^{-1}, while the hydroxyl groups of molecular water bending and C═C stretching indicated absorption peaks at 1620 cm^{-1}. The carboxyl group, phenolic C—O—H, and C—O stretching vibrations in the epoxy were detected at 1375 cm^{-1}, 1220 cm^{-1}, and 1045 cm^{-1}, respectively.[10,38] A distinct and drastic decrease in intensity of absorption peaks was observed at C═O (1750 cm^{-1}), C═C (1620 cm^{-1}), C—O—H (1220 cm^{-1}), and C—O (1045 cm^{-1}) that corresponds to oxygen functional groups contributed by the reduction of GO. Meanwhile, TiO_2 NPs show wide peaks at 3350 and 1630 cm^{-1} which correspond to the O—H group of water, whereas the wide and broad peaks 500-900 cm^{-1} are attributed to the stretching vibration of Ti—O—Ti and Ti—O—C bonds.[11,39] Fig. S4 in the supplementary material depicts the magnified FTIR spectra.[29]

The chemical elemental species of the prepared samples are shown in Figs. 4(a)-4(d). From Fig. 4(a), C 1s devolved into four peaks at 284.8, 286.6, 287.8, and 289.0 eV were seen. The corresponding binding energies signified to different functional groups of C—C and C—O in hydroxyl or epoxy forms, C═O and COOH, respectively.[20,40] A significant decrease of C—O and C═O peaks of C 1s observed in sample (RGO-Ag/TiO_2) indicating the considerable elimination of oxygen containing groups during the hydrothermal treatment (Fig. 4(b)). Fig. 4(c) exhibited two distinct peaks at 529.08 eV and 530.89 eV indicating the presence of Ti—O—Ti and Ti—O—C bonds, respectively.[11] The presence of Ag NPs was clearly shown in Fig. 4(d). Fig. S5 in the supplementary material illustrates the Ti core level obtained from the XPS spectrum.[29]

In analyzing the light absorption of the synthesized materials, UV-visible absorption spectroscopy analysis was executed and shown in Fig. 5(A). A considerable red shift towards visible light region is clearly observed for RGO-TiO_2 and RGO-Ag/TiO_2 indicating narrow bandgap energy with the introduction of RGO. This significant shift ascertains the incorporation of RGO in the composite

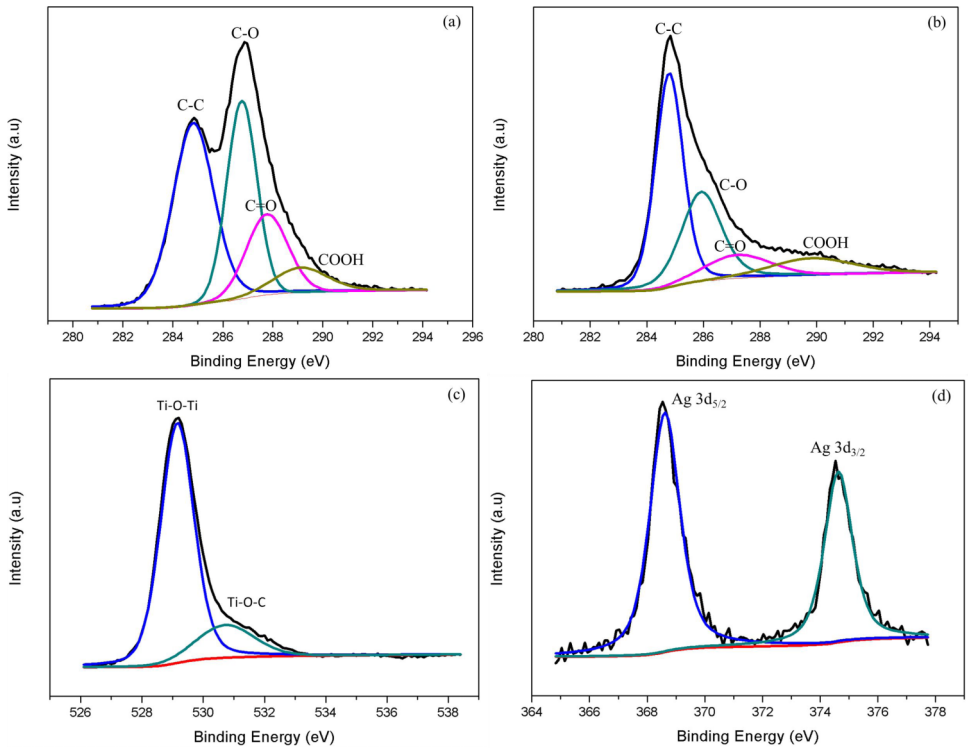

FIG. 4. Chemical elemental species spectra of (a) C 1s of GO, (b) C 1s of RGO-Ag/TiO_2, (c) O 1s, and (d) Ag 3d.

through Ti—O—C bond.[11,41,42] Further enhancement in the visible light region at ~460 nm can be seen after the incorporation of Ag NPs into the composite (RGO-Ag/TiO_2).[16,25,43] The existence of Ag NPs on the surface of TiO_2 significantly oscillated the dielectric constant surrounding the matrix leading to the visible light absorption.[16] Fig. 5(B) reveals the calculated (Kulbeka-Munk equation) bandgap energy for the prepared photocatalysts. It was found that after the incorporation of RGO, the bandgap energy of TiO_2 was tuned to 2.9 eV. The reduction in bandgap was attributed to the formation of Ti—O—C bond, where the electrons on the surface of TiO_2 are bonded with unpaired π-electrons and leading to a shift upwards the valence band edge.[11] The observed phenomenon enhanced the RGO-Ag/TiO_2 with a notable visible light performance.

The photoluminescence spectra for the prepared photocatalysts are portrayed in Fig. 6(A). It is well proven from the spectrum that the deposition of RGO and Ag NPs drastically prolonged the lifetime of the charge carriers. This is owing to the trapping of the photo-excited electrons and high

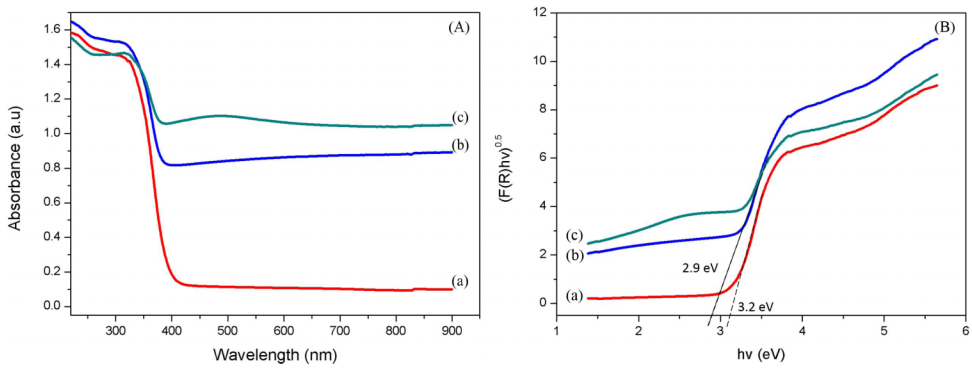

FIG. 5. (A) UV-visible absorption spectra and (B) calculated bandgap energies of (a) TiO_2, (b) RGO-TiO_2, and (c) RGO-Ag/TiO_2.

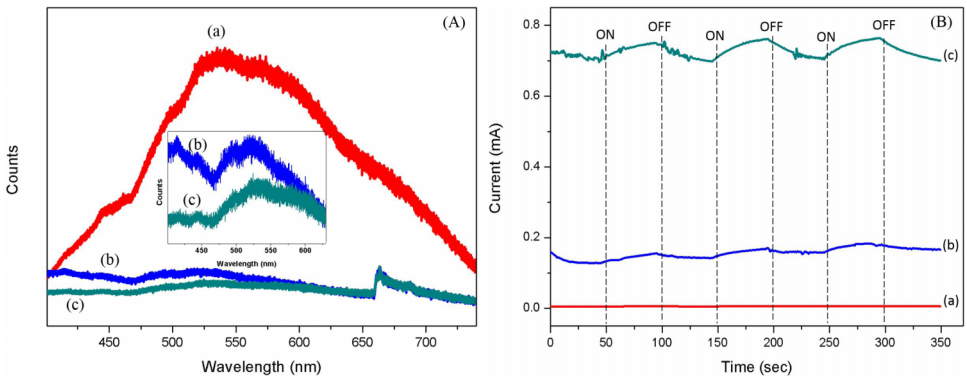

FIG. 6. (A) Photoluminescence spectra and (B) photocurrent transient responses of (a) TiO_2, (b) RGO-TiO_2, and (c) RGO-Ag/TiO_2.

charge carrier mobility of RGO.[25,44] A more active separation of electron-hole pairs was observed after incorporation of Ag NPs. This resulted from the effective electrons transfer from TiO_2—Ag NPs-RGO. Transient photocurrent responses were studied to provide additional evidence for the separation of the photoelectrons and holes of the prepared photocatalysts. The responses were recorded over several cycles of on-off visible light irradiation as shown in Fig. 6(B). The higher photocurrent possessed by RGO-Ag/TiO_2 as compared to rest demonstrated the higher efficiency of the charge separation in the composite.

Fig. 7 describes the visible light utilisation ability of prepared photocatalysts. It is evident that BPA is very stable and possesses poor photosensitizing nature where almost zero degradation was obtained in the presence of visible light alone. An improved comprehensive degradation was achieved by RGO-TiO_2 for BPA compounds within 6 h. The attained improvement on visibility was attributed to the enhancement of the significant red shift through Ti—O—C bond. The bond formation was apprised by the oxygen sites in the TiO_2 lattice that are replaced by carbon atoms.[45] Therefore, when visible light illumination is enabled, the photoexcitation was initiated in the O-2p orbital to Ti-3d orbital and leaves behind holes at the O-2p state with a very high redox potential.[11] This high redox potential catalyse the reaction between holes and H_2O leading to the formation of active $^{\bullet}OH$ radicals. The high redox potential also allows easy movement of generated electrons from TiO_2 to RGO due to work functions of RGO (4.4 eV) that underlay beneath the conduction band of TiO_2 (4.2 eV).[27] These electrons then react with adsorbed O_2 to form superoxide anion radical ($^{\bullet}O_2^-$). Thus, it prolongs the lifetime of electron and hole pairs.[27,44]

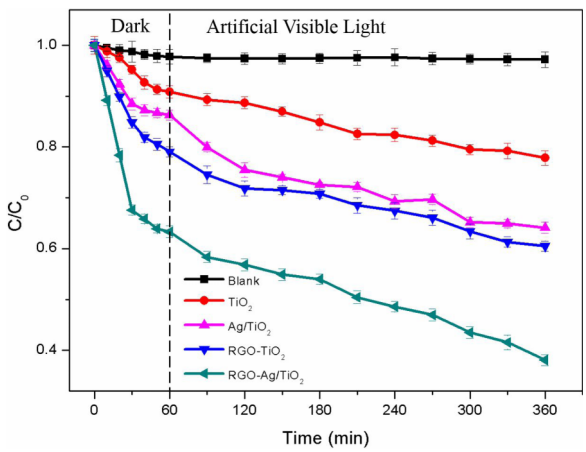

FIG. 7. Photocatalytic activity of Bisphenol A.

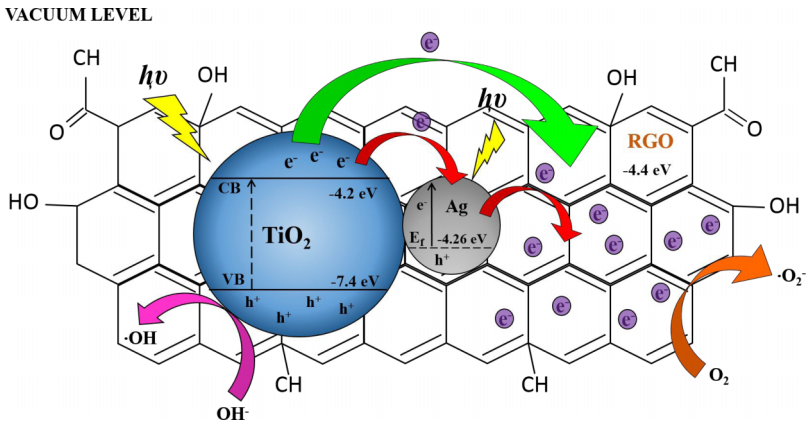

FIG. 8. Excitation mechanism of RGO-Ag/TiO_2 photocatalyst under visible light irradiation.

A good photodegradation efficiency of 40.0% was observed for the RGO-Ag/TiO_2 than that of RGO-TiO_2 (25.2%), Ag/TiO_2 (24.9%), and TiO_2 (14.4%). It is well evident that this greater efficiency was also attributed to the inclusion of Ag NPs into the composite. The Ag NPs with a characteristic of negative work function (4.26 eV) stimulated the ability to capture the photogenerated electrons of TiO_2. When these NPs get intimated with RGO, it further transfers the electrons to the surface of RGO. Hence, it further suppresses recombination and thereby increasing the overall photocatalysis performance. Moreover, the LSPR phenomenon triggered by the noble metal also well contributed for the visible light enhancement. The presence of visible light excited the Ag surface plasmon and this collective electron oscillation generates high concentration of energetic electrons at its surface. The RGO surface then quickly transports those electrons from Ag surface through extended π-conjugation structure.[46] This effective movement of electrons from Ag to RGO surface prolongs the life span of the charge carriers.[46] The excess formation of electrons through Ag also reacts with surface absorbed oxygen forming superoxide anion radical ($^{\bullet}O_2^-$), whereas the holes form active radicals ($^{\bullet}OH$) by reacting with H_2O molecule. The immense production of $^{\bullet}OH$ radicals triggered through respective mechanism contributed for enhanced suppression of electron-holes recombination. The interaction of photocatalyst with BPA under visible light irradiation is depicted in Fig. 8.

In conclusion, visible light promoted composite TiO_2 was successfully achieved with the support of Ag and RGO. Each of them had their own way of characteristics for triggering the potential TiO_2 towards the visible spectrum. The RGO anchored the TiO_2 through a stable bonding that enhanced the visible light utilization progressively. The binding promoted ease electron mobilisation between titania and RGO. The Ag supported the composite through an energetic LPSR phenomenon well supported for the enriched production of hydroxyl radical and delayed the union of electrons and holes. The accomplishment of synergised effect of RGO and Ag demonstrated an excellent photocatalysis by degrading BPA under visible light irradiation. Thus, the present study exhibited significant contributions of the each element in the composites for the enhancement of titania towards utilising non-renewable energy resource for sustainable treatment.

The first author is grateful to University of Malaya for the Bright Spark Fellowship. This work was supported by Fundamental Research Grant Scheme, FRGS (No. FP051-2013B) and Postgraduate Research Grant, PPP (No. PG022-2013A). The corresponding author would like to thank Professor Dr. Sharifah Bee Head, Nanotechnology & Catalysis Research Center (NANOCAT), University of Malaya for the transient photocurrent analysis.

[1] P. Guerra, M. Kim, S. Teslic, M. Alaee, and S. Smyth, J. Environ. Manage. **152**, 192–200 (2015).
[2] Y. Huang, C. Wong, J. Zheng, H. Bouwman, R. Barra, B. Wahlström, L. Neretin, and M. Wong, Environ. Int. **42**, 91–99 (2012).
[3] L. Luo, Y. Yang, M. Xiao, L. Bian, B. Yuan, Y. Liu, F. Jiang, and X. Pan, Chem. Eng. J. **262**, 1275–1283 (2015).
[4] N. Lu, Y. Lu, F. Liu, K. Zhao, X. Yuan, Y. Zhao, Y. Li, H. Qin, and J. Zhu, Chemosphere **91**(9), 1266–1272 (2013).
[5] P.-S. Yap, T.-T. Lim, M. Lim, and M. Srinivasan, Catal. Today **151**(1), 8–13 (2010).

[6] B. Czech and W. Buda, Environ. Res. **137**, 176–184 (2015).
[7] U. I. Gaya and A. H. Abdullah, J. Photochem. Photobiol., C **9**(1), 1–12 (2008).
[8] H. A. Le, S. Chin, and J. Jurng, Powder Technol. **225**, 167–175 (2012).
[9] B. Elgh, N. Yuan, H. S. Cho, D. Magerl, M. Philipp, S. V. Roth, K. B. Yoon, P. Müller-Buschbaum, O. Terasaki, and A. E. Palmqvist, APL Mater. **2**(11), 113313 (2014).
[10] L.-L. Tan, W.-J. Ong, S.-P. Chai, and A. R. Mohamed, Nanoscale Res. Lett. **8**(1), 465 (2013).
[11] S. Umrao, S. Abraham, F. Theil, S. Pandey, V. Ciobota, P. K. Shukla, C. J. Rupp, S. Chakraborty, R. Ahuja, and J. Popp, RSC Adv. **4**(104), 59890–59901 (2014).
[12] J. Yu, Q. Xiang, and M. Zhou, Appl. Catal., B **90**(3), 595–602 (2009).
[13] J. Fang, L. Yin, S. Cao, Y. Liao, and C. Xue, Beilstein J. Nanotechnol. **5**(1), 360–364 (2014).
[14] L. Guo, D. Jing, M. Liu, Y. Chen, S. Shen, J. Shi, and K. Zhang, Beilstein J. Nanotechnol. **5**(1), 994–1004 (2014).
[15] H. Chen and L. Wang, Beilstein J. Nanotechnol. **5**(1), 696–710 (2014).
[16] K. H. Leong, B. L. Gan, S. Ibrahim, and P. Saravanan, Appl. Surf. Sci. **319**, 128–135 (2014).
[17] S. Kuriakose, V. Choudhary, B. Satpati, and S. Mohapatra, Beilstein J. Nanotechnol. **5**(1), 639–650 (2014).
[18] K. H. Leong, H. Y. Chu, S. Ibrahim, and P. Saravanan, Beilstein J. Nanotechnol. **6**(1), 428–437 (2015).
[19] M. C. Mathpal, A. K. Tripathi, P. Kumar, R. Balasubramaniyan, M. K. Singh, J. S. Chung, S. H. Hur, and A. Agarwal, Phys. Chem. Chem. Phys. **16**(43), 23874–23883 (2014).
[20] D. Wang, X. Li, J. Chen, and X. Tao, Chem. Eng. J. **198**, 547–554 (2012).
[21] N. Zhang, Y. Zhang, and Y.-J. Xu, Nanoscale **4**(19), 5792–5813 (2012).
[22] Y. Tang, S. Luo, Y. Teng, C. Liu, X. Xu, X. Zhang, and L. Chen, J. Hazard. Mater. **241**, 323–330 (2012).
[23] Q. Xiang, J. Yu, and M. Jaroniec, Chem. Soc. Rev. **41**(2), 782–796 (2012).
[24] Z. Wu, H. Zhong, X. Yuan, H. Wang, L. Wang, X. Chen, G. Zeng, and Y. Wu, Water Res. **67**, 330–344 (2014).
[25] M. S. A. S. Shah, K. Zhang, A. R. Park, K. S. Kim, N.-G. Park, J. H. Park, and P. J. Yoo, Nanoscale **5**(11), 5093–5101 (2013).
[26] S. Liu, H. Sun, S. Liu, and S. Wang, Chem. Eng. J. **214**, 298–303 (2013).
[27] Y. Wang, Y. Tang, Y. Chen, Y. Li, X. Liu, S. Luo, and C. Liu, J. Mater. Sci. **48**(18), 6203–6211 (2013).
[28] W. S. Hummers, Jr. and R. E. Offeman, J. Am. Chem. Soc. **80**(6), 1339 (1958).
[29] See supplementary material at http://dx.doi.org/10.1063/1.4926454 for preparation of GO, schematic preparation of RGO-Ag/TiO_2, FESEM and HRTEM images of TiO_2 and Ag/TiO_2, magnified image of FT-IR and XPS spectra of Ti 2p.
[30] K. H. Leong, P. Monash, S. Ibrahim, and P. Saravanan, Sol. Energy **101**, 321–332 (2014).
[31] Z. Chen, L. Fang, W. Dong, F. Zheng, M. Shen, and J. Wang, J. Mater. Chem. A **2**(3), 824–832 (2014).
[32] D. Chen, Q. Chen, L. Ge, L. Yin, B. Fan, H. Wang, H. Lu, H. Xu, R. Zhang, and G. Shao, Appl. Surf. Sci. **284**, 921–929 (2013).
[33] J. Zhang, Z. Xiong, and X. Zhao, J. Mater. Chem. **21**(11), 3634–3640 (2011).
[34] W.-S. Wang, D.-H. Wang, W.-G. Qu, L.-Q. Lu, and A.-W. Xu, J. Phys. Chem. C **116**(37), 19893–19901 (2012).
[35] C. Zeng, M. Guo, B. Tian, and J. Zhang, Chem. Phys. Lett. **575**, 81–85 (2013).
[36] J. Yang, C. Tian, L. Wang, and H. Fu, J. Mater. Chem. **21**(10), 3384–3390 (2011).
[37] M. Zhu, P. Chen, and M. Liu, ACS Nano **5**(6), 4529–4536 (2011).
[38] L. C. Sim, K. H. Leong, S. Ibrahim, and P. Saravanan, J. Mater. Chem. A **2**(15), 5315–5322 (2014).
[39] Y. Liu, K. Chen, M. Xiong, P. Zhou, Z. Peng, G. Yang, Y. Cheng, R. Wang, and W. Chen, RSC Adv. **4**(82), 43760–43765 (2014).
[40] H. Zhang, X. Fan, X. Quan, S. Chen, and H. Yu, Environ. Sci. Technol. **45**(13), 5731–5736 (2011).
[41] Y. Yang, E. Liu, H. Dai, L. Kang, H. Wu, J. Fan, X. Hu, and H. Liu, Int. J. Hydrogen Energy **39**(15), 7664–7671 (2014).
[42] W. Ren, Z. Ai, F. Jia, L. Zhang, X. Fan, and Z. Zou, Appl. Catal., B **69**(3), 138–144 (2007).
[43] Y. Wen, H. Ding, and Y. Shan, Nanoscale **3**(10), 4411–4417 (2011).
[44] P. Wang, Y. Tang, Z. Dong, Z. Chen, and T.-T. Lim, J. Mater. Chem. A **1**(15), 4718–4727 (2013).
[45] F. Dong, H. Wang, and Z. Wu, J. Phys. Chem. C **113**(38), 16717–16723 (2009).
[46] S. K. Bhunia and N. R. Jana, ACS Appl. Mater. Interfaces **6**(22), 20085–20092 (2014).